Available online at www.sciencedirect.com

ScienceDirect

Procedia Structural Integrity 14 (2019) 499–506

Structural Integrity Procedia

www.elsevier.com/locate/procedia

2nd International Conference on Structural Integrity and Exhibition 2018

Influence of axial constraint on the creep and plastic deformation of a cladding tube

Shekhar Suman[a]*, Sivasambu Mahesh[a]

[a]*Department of Aerospace Engineering, Indian Institute of Technology, Madras, Chennai 600036, India*

Abstract

Tube ballooning of axially confined tubes under increasing thermal loading is studied using a finite element model in an austenitic stainless steel, alloy D9. The model accounts for thermal, plastic and creep deformation of the tube. It is shown that (i) axial restrains can trigger the onset of plasticity, and (ii) activation of plasticity during the thermomechanical loading can significantly reduce the time for the development of large ballooning strains.

Keywords: Ballooning; LOCA; Nuclear fuel cladding; D9 alloy; Johnson-Cook plasticity model; creep

1. Introduction

Nuclear fuel cladding encloses the nuclear fuel pellets and acts as a protective shield between fuel pellet and coolant. Clad tube ballooning in the Loss of Coolant Accident (LOCA) scenario is an important failure mechanism. Ballooning is deleterious because it restricts the coolant flow between the cladding tubes, and thereby reduces heat removal. The internal pressure and temperature of the clad tube will thus rise because of decay heat of the nuclear fuel. This may lead to thinning of the tube walls and culminate with burst. Tube bursting will contaminate the coolant fluid. Ballooning of axially unrestrained cladding tubes has been extensively investigated in the literature (Neitzel and Rossinger (1980), Manngard and Massih (2011), Massey et al. (2016) and Khan and Pathak (2014)).

* Corresponding author. Tel.: +91-7358185615
E-mail address: ae15s010@smail.iitm.ac.in

10.1016/j.prostr.2019.05.060

These works have focused on the ballooning behavior of axially unconstrained tubes. In this case, ballooning is primarily driven by creep deformation. A number of causes leading to axial restraint on the tube during normal operation have been enumerated by Pickman (1975). Some of them are: (i) axial growth of the clad tube during service, due to irradiation and ratcheting, (ii) accumulation of crud at the spacer grid, and (iii) accelerated corrosion between the fuel pin and the spacer grid. Additionally, unforeseen circumstances of the accident scenario may also introduce axial restraint on the fuel pin. This paper deals with the study of the ballooning behavior of an axially constrained clad tube made of the austenitic stainless steel alloy, D9. In the presence of the axial constraint, both plasticity and creep may contribute to the deformation of the tube. Hence, both mechanisms are accounted for in the present study. A finite element model of the tube incorporating these deformation mechanisms in a coupled thermomechanical framework is constructed. The key question presently considered is whether allowing the additional accommodation mechanism of plasticity reduces the creep rate, and thereby enhances the time taken for creep-dominated ballooning, or whether plasticity compounds the creep rate, and reduces the time to ballooning.

Nomenclature

LOCA	Loss of Coolant Accident
σ_{eq}	Von-Mises equivalent stress
$\varepsilon_{p,eq}$	Equivalent plastic strain
$\varepsilon_{c,eq}$	Equivalent creep strain
T_m	Melting temperature
T_{ref}	Reference temperature for Johnson-Cook plasticity model
Q	Activation energy
R	Gas constant
A,B,n,m	Johnson-Cook plasticity parameters
A_0	Coefficient of Norton power law for creep
b	Stress exponent for Norton power law for creep

2. Geometry and Modeling

2.1. Geometry

The geometry of D9 alloy clad tube used for PFBR (Prototype Fast Breeder Reactor) application, as reported by Sarkar et al. (2018) is presently considered. Its outer diameter and thickness are 6.6 mm and 0.45 mm respectively. The length considered for the analysis is 300 mm, which is much longer than the diameter of the tube. In a perfect model tube, localized deformations will not occur. To initiate localized deformation a defect is placed into the model. This defect is in the form of an axisymmetric notch and is created at the mid length at the inner surface of the tube with a depth of one-tenth of the thickness. The length of the notch is assumed to be three times the thickness for this study. A sketch of the model geometry is shown in Fig. 1(a).

2.2. ABAQUS Modeling

An axisymmetric finite element model is created using ABAQUS (ABAQUS 6.14 documentation (2014)) to simulate the tube ballooning with axial constraint. Meshing is done so that there are 10 first order quadrilateral elements (CAX4T) through the thickness of size 0.05 mm as shown in Fig. 1(b). Pressure is applied to the inner surface of the cylindrical tube with a magnitude of 6.5 MPa, to mimic the conditions detailed by Sarkar et al. (2018). Temperature boundary condition on the outer surface of the cylinder increases linearly from 323 K to 1173 K in 3180 s. In the next 1020 s, the temperature increases linearly from 1173 K to 1223 K, and over the subsequent 420 s, the temperature is kept constant. The imposed temperature profile again follows the experimental study of Sarkar et al. (2018), and is shown in Fig. 2. The model is rigidly restrained in the axial direction. A coupled thermal-plastic-creep analysis is performed. Non-linear changes in the geometry during the simulation are accounted for.

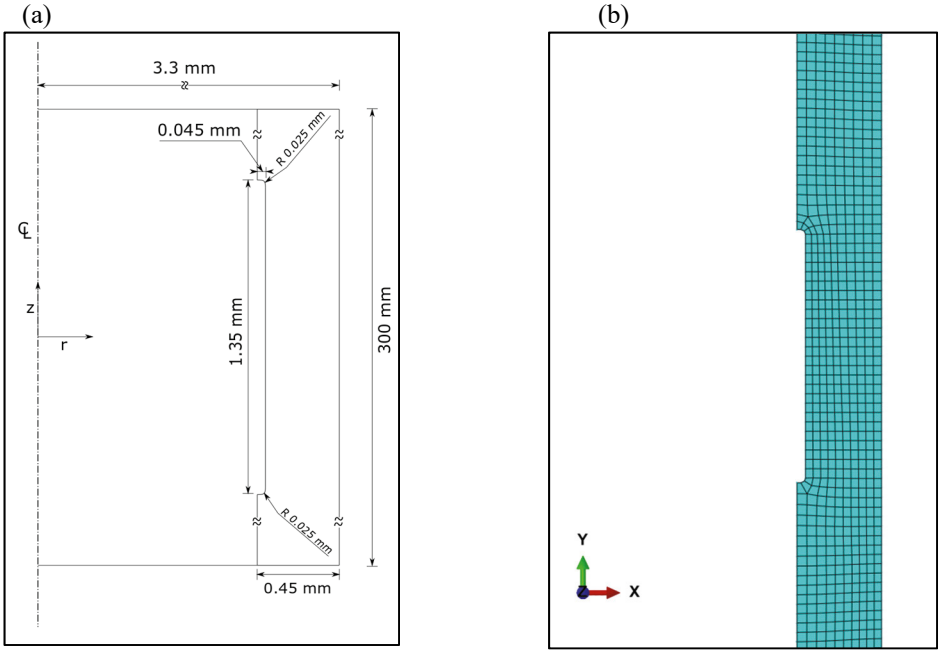

Fig. 1. (a) Geometry details of the ABAQUS model; (b) ABAQUS meshed model detail

The material property of 316 stainless steel is used in the analysis wherever the data for D9 alloy is not available. These material properties are taken from the I.N.C.O. databook (1968) and European Standard EN 10088-1 and are shown in Table 1 and in Fig. 3. To incorporate plasticity and creep phenomena in the model, Johnson and Cook (1983) plasticity model and Norton power law for creep is used. Parameter values of these two models are detailed in section 3.

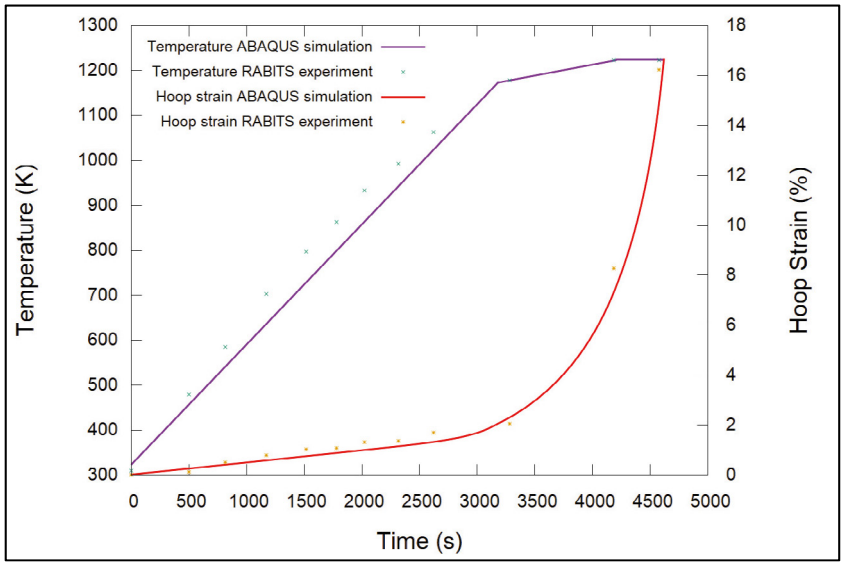

Fig. 2. Comparison of finite element predictions of temperature and hoop strain against the experimental measurements by Sarkar et al. (2018).

Table 1. Material properties used in the analysis

Material Property	Value
Conductivity	15 W/mK
Density	8000 kg/m^3
Thermal expansion coefficient	1.8e-5 K^{-1}
Specific heat	500 J/kgK
Poisson's ratio	0.27

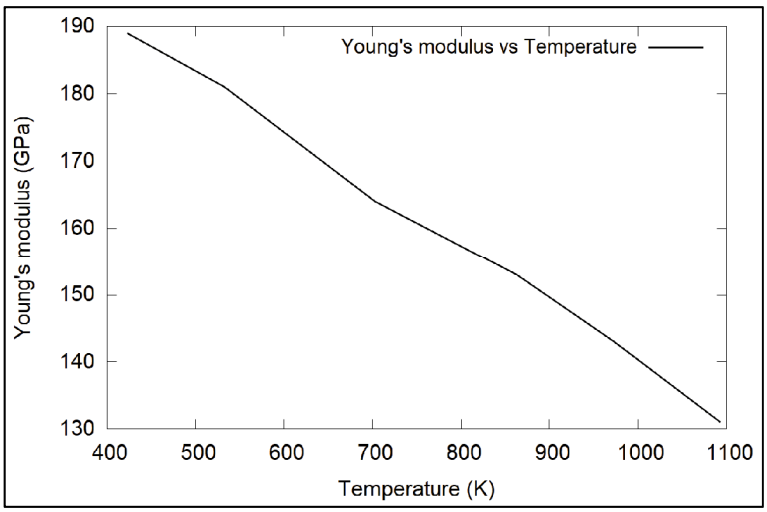

Fig. 3. Variation of Young's modulus with temperature

3. Plasticity and Creep Parameters

3.1. Johnson-Cook (JC) parameters

The cladding material is assumed to obey J_2 plasticity and hardening following the Johnson and Cook (1983) law:

$$\sigma_{eq} = \left(A + B\varepsilon_{p,eq}^{n}\right)\left(1 - \left(\frac{T - T_{ref}}{T_m - T_{ref}}\right)^{m}\right)$$

The parameters of the hardening law, for the present D9 material, are determined by fitting the tensile stress-strain data reported by Samantaray et al. (2009) in the temperature range of 1073 K to 1473 K. Since their specimen were annealed to begin with, and since the cladding tube used for ballooning tests by Sarkar et al. (2018) were 20% cold-worked, only the stress-strain measurements of Samantaray et al. (2009) beyond the strain value of 20% were considered. The Johnson-Cook parameters *A, B, n* and *m* giving the best fit to the data for temperature range of 1073 K to 1223 K are shown in

Table 2. Lacking data for lower temperatures than 1073 K, the mechanical response is assumed to follow the response at 1073 K over this range. This assumption is conservative.

Table 2. Johnson-Cook parameter values

A (MPa)	*B (MPa)*	*n*	*m*	T_m *(K)*	T_{ref} *(K)*
291.09	119.98	0.857	0.465	1673	1073

3.2. Creep constants

The power law given by Norton (1929) is used to include the creep effect in the finite element model:

$$\dot{\varepsilon}_{c,eq} = A_0 \sigma_{eq}^{b} \exp\left(-\frac{Q}{RT}\right)$$

The creep parameters for temperature range of 1123 K to 1223 K are not available in the literature for D9 SS alloy. Value of stress exponent b is taken as 9, which is reported by Latha et al. (2008) at 973 K. For other constants, A_0 and Q, the values are chosen so that finite element predictions of the evolution of hoop strain matches with the measurements of Sarkar et al. (2018) on axially unrestrained tubes. The values of Q and A_0 thus obtained are 185 kJ/mol and 1.73e-11 $MPa^{-b}s^{-1}$ respectively. The hoop strain predicted by the finite element calculation is compared with the experimental measurements of Sarkar et al. (2018) in Fig. 2. It is clear that excellent coincidence between the two is obtained, which is taken as a validation of the model parameters.

4. Results

Simulations of tube ballooning with the material parameters obtained in the preceding section, but with their axial ends rigidly restrained are conducted for the temperature profile shown in Fig. 2. Plastic strain is observed in the clad tube in the initial heating stage at about 660 s (Fig. 4). Even though plasticity starts early in the heating process, and precedes the activation of creep deformation, creep overtakes plasticity soon and within 1000 s, the plastic strain becomes constant due to the creep relaxation of stresses. Thereafter, the creep component of hoop strain rises and eventually results in ballooning after about 4000 s of heating.

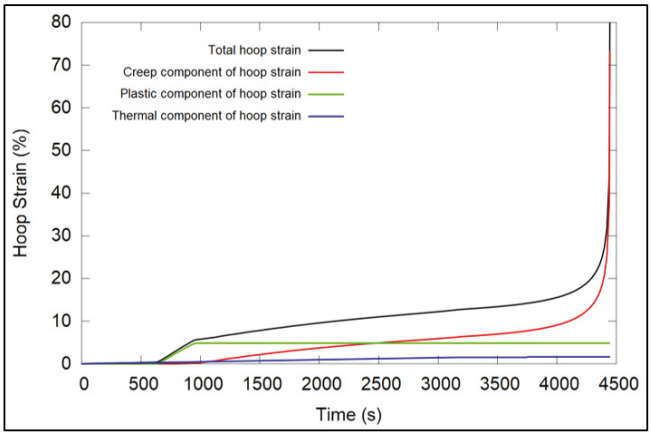

Fig. 4. Evolution of hoop strain components with time in an axially restrained tube. Contributons from thermal strains, plastic strains, and creep strains are shown separately.

To understand how plasticity will affect the ballooning time, plasticity is deactivated in the finite element model and the evolution of hoop strain with time is studied. Fig. 5 compares the hoop strain evolution predicted by the two models, “model with creep and plasticity” and “model with creep alone”. When plasticity is present, the hoop strain quickly rises to 5% within 300 s, while the rate of creep strain is relatively slow at lower temperatures. At higher temperature (i.e. temperature greater than 1173 K) creep strain rate becomes significant and results in ballooning for both “model with creep and plasticity” and “model with creep alone” models. For each hoop strain level, the time difference between with and without plasticity models is shown in Fig. 6. It is seen that the time difference is greatest (about 2000 s) at about 8% hoop strain.

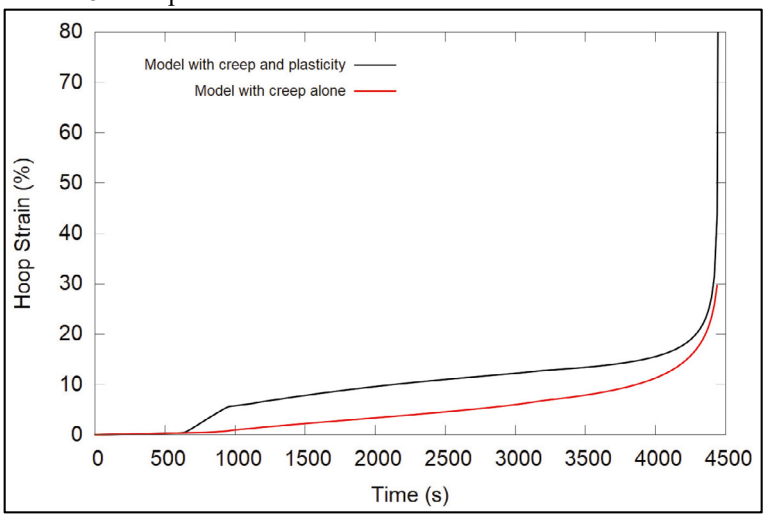

Fig. 5. Hoop strain evolution with time without and without plasticity.

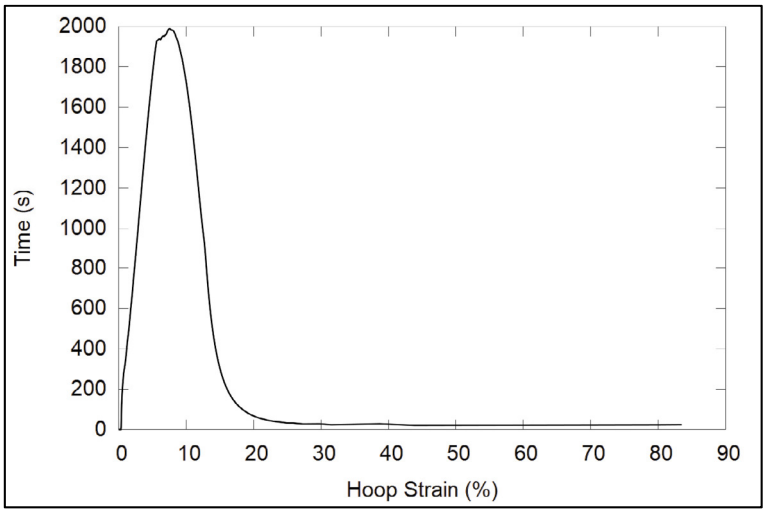

Fig. 6. Time difference between “creep with plasticity model” and “creep only model” to attain given hoop strain

5. Discussion

The foregoing result that the activation of plasticity accelerates the process of ballooning is counter-intuitive. This is because, it was expected that in a homogeneously deforming notch section, plastic strains will accommodate

a part of the thermal strains, and thereby relax the stresses, resulting in smaller creep-rates in the material. This, it was expected, will delay the onset of large ballooning strains. Instead, it is found that plastic flow accelerates tube ballooning by creep.

The reason behind the present observation is that the deformation of the tube is highly inhomogeneous through the thickness. As shown in Fig. 7, there is a through-thickness gradient in the stresses. This gradient develops due to bulging of the tube. The greatest radial displacement due to bulging occurs at the mid-section of the notched region in the model. Tube bulging is accommodated initially by plasticity. It induces larger stresses at the inner diameter, than at the outer diameter, as show in in Fig. 7. These stresses, in turn, activate creep deformation, first the inner diameter, and propagating outward with time. After large times, creep deformation has relaxed the stresses throughout the tube thickness.

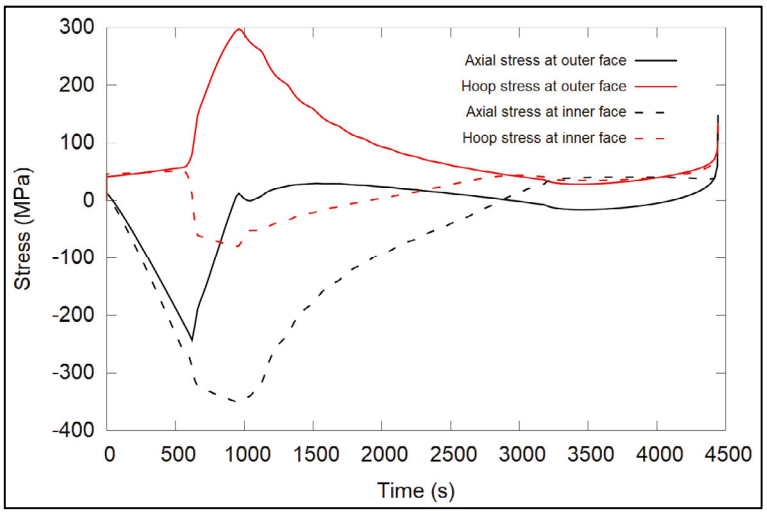

Fig. 7. Axial and hoop stress evolution with time at inner and outer surface of clad tube for creep with plasticity model

In summary, plasticity accelerates tube ballooning by creep deformation because the ballooned section undergoes inhomogeneous bulging deformation.

6. Conclusion

The present study shows that the presence of plasticity can significantly reduce the ballooning time for the clad tube in the axially constraint scenario. When plasticity occurs in the model the hoop strain quickly increases but within a few hundred seconds because of stress relaxation due to creep, no further increase in the plastic strain occurs. The difference of time to balloon in the two models is significant for the initial ballooning stage (<10%). In the later stages of ballooning the contribution of creep is much larger than plasticity for the D9 alloy of present interest.

References

ABAQUS, 2014. 6.14 Documentation. Dassault Systemes Simulia Corporation.

Databooks, I.N.C.O., 1968. Austenitic chromium-nickel stainless steels–engineering properties at elevated temperatures. The International Nickel Company.

EN 10088-1, 2005. Stainless steels – Part 1: List of stainless steels. CEN.

Johnson, G.R. and Cook, W.H., 1983. A constitutive model and data for metals subjected to large strains, strain rates, and high pressures. In Proceedings of the 7th International Symposium On Ballistics, 541-547.

Khan, M.K., Pathak, M., Suman, S., Deo, A. and Singh, R., 2014. Burst investigation on zircaloy-4 claddings in inert environment. Annals of Nuclear Energy 69, 292-300.

Latha, S., Mathew, M.D., Parameswaran, P., Rao, K.B.S. and Mannan, S.L., 2008. Thermal creep properties of alloy D9 stainless steel and 316 stainless steel fuel clad tubes. International Journal of Pressure Vessels and Piping 85(12), 866-870.

Manngard T., Massih A.R., 2011. Modelling and simulation of reactor fuel cladding under loss-of-coolant accident conditions. Journal of nuclear science and technology 48(1), 39–49

Massey C.P., Terrani K.A., Dryepondt S.N., Pint B.A., 2016. Cladding burst behavior of fe-based alloys under loca. Journal of Nuclear Materials 470, 128–138

Neitzel H.J., Rossinger H., 1980. The development of a burst criterion for zircaloy fuel cladding under loca conditions. Tech. rep., Atomic Energy of Canada Ltd.

Norton, F.H., 1929. The creep of steel at high temperatures. McGraw-Hill, New York.

Pickman, D.O., 1975. Interactions between fuel pins and assembly components. Nuclear Engineering and Design 33(2), 125-140.

Samantaray, D., Mandal, S., Borah, U., Bhaduri, A.K. and Sivaprasad, P.V., 2009. A thermo-viscoplastic constitutive model to predict elevated-temperature flow behaviour in a titanium-modified austenitic stainless steel. Materials Science and Engineering: A 526(1-2), 1-6.

Sarkar, R., Kumar, R.S., Jalaldeen, S., Sharma, A.K. and Velusamy, K., 2018. Ballooning in fuel clad: The first of its kind approach for its investigation in fast reactors. International Journal of Pressure Vessels and Piping 160, 24-33.